1	Hemolymph viscosity in hawkmoths and its implications for hovering flight				
2	Artis Brasovs ¹ , Alexandre V. Palaoro ¹ , Pavel Aprelev ¹ , Charles E. Beard ² , Peter H. Adler ²				
3	and Konstantin G. Kornev ^{1,3*}				
4	¹ Department of Materials Science and Engineering, Clemson University, Clemson, South				
5	Carolina, USA, 29634				
6	² Department of Plant and Environmental Sciences, Clemson University, Clemson, South				
7	Carolina USA, 29634				
8	³ Department of Biological Sciences, Clemson University, Clemson, South Carolina, USA				
9	29634				
10	*Corresponding author: Konstantin G. Kornev, kkornev@clemson.edu				

ABSTRACT

Viscosity determines the resistance of hemolymph flow through the insect body. For flying insects, viscosity is a major physiological parameter limiting flight performance by controlling the flow rate of fuel to the flight muscles, circulating nutrients, and rapidly removing metabolic waste products. The more viscous the hemolymph, the greater the metabolic energy needed to pump it through confined spaces. By employing Magnetic Rotational Spectroscopy with nickel nanorods, we showed that viscosity of hemolymph in resting hawkmoths (Sphingidae) depends on wing size non-monotonically. Viscosity increases for small hawkmoths with high wingbeat frequencies, reaches a maximum for middle-sized hawkmoths with moderate wingbeat frequencies, and decreases in large hawkmoths with slower wingbeat frequencies but greater lift. Accordingly, hawkmoths with small and large wings have viscosities approaching that of water, whereas hawkmoths with mid-sized wings have more than twofold greater viscosity. The metabolic demands of flight correlate with significant changes in circulatory strategies via modulation of hemolymph viscosity. Thus, the evolution of hovering flight would require fine-tuned viscosity adjustments to balance the need for the hemolymph to carry more fuel to the flight muscles while decreasing the viscosu dissipation associated with its circulation.

Keywords; Biomechanics, hemolymph, metabolism, flight, Lepidoptera, Sphingidae

INTRODUCTION

The enormous evolutionary diversity of insects is tied to special properties of their hemolymph. Its functions range from tissue irrigation and materials transport to wound healing and protection against microbial invasion. These functions are connected through physicochemical phenomena[1–5].

Hemolymph of butterflies and moths (Lepidoptera) typically contains fewer cells (hemocytes) than that of their larvae; consequently, the transport properties of the hemolymph of adults should be distinguishable from those of larvae[6,7]. Viscosity characterizes the resistance of hemolymph to flow: the more viscous the hemolymph, the higher the pressure gradient that must be applied to push it through confined spaces (e.g., the dorsal vessel) [8]. To generate this pressure gradient, greater muscular action is demanded from the insect and, hence, greater metabolic energy is needed to do this mechanical work. For flying insects, viscosity is a major physiological parameter limiting flight performance by controlling the flow rate of fuel to the flight muscles, circulating nutrients, and rapidly removing metabolic waste products[9–12].

Insufficient fuel is stored in the flight muscles[13–15]. The main metabolic fuel in migrating butterflies and hawkmoths, therefore, switches from carbohydrate to lipid soon after the commencement of a long flight[16]. Lipid fuel is stored mostly in the fat body and has to be chemically extracted and transported to the flight muscles[17–21]. In aqueous hemolymph, hydrophobic lipids cannot be dissolved at high concentrations. Insects, therefore, have developed special lipoprotein nanoparticles, lipophorins[20], that shuttle various lipids between the fat body and the flight muscles[17–21]. These large lipoprotein nanoparticles, together with other organic and inorganic constituents, occupy about 10% of hemolymph volume[3,22]. Hemolymph, therefore, can be considered a colloidal suspension.

The viscosity of any suspension is greater than that of the carrying liquid[23], water in the case of hemolymph. Thus, the greater the concentration of lipoprotein particles, the greater the expected viscosity. Hemolymph lipid and lipophorin levels increase significantly during flight[20] in species such as *Danaus plexippus*[24] and *Manduca sexta*[25]. Butterflies and moths with greater lipid and lipophorin levels and hence with greater viscosity must generate stronger pressure gradients to pump hemolymph through the body, wings, and appendages by generating stronger heart beats[26] or forcibly contracting and expanding hemolymph conduits with their muscles. The dilemma for a required increase in concentration of fuel and a decrease of viscous dissipation of circulating hemolymph by flying insects sets the scene for the development of different physiological strategies in the evolutionary diversification of species.

Despite the importance of viscosity for insect function, data on viscous properties of hemolymph are lacking. The lack of viscosity data hinders rigorous analysis of the energy demands for flying insects. To fill this gap, we characterized hemolymph viscosity of the adults of 14 species of Lepidoptera by applying Magnetic Rotational Spectroscopy (MRS) with magnetic nanorods[7,27,28]. To put the viscosity data into the context of hemolymph circulation, we used micro-computed tomography scans to characterize the structure of the thoracic hemolymph pathways of hawkmoths. This characterization allowed us to couple hemolymph transport properties to the morphology, providing an estimate of the size constraints of available hemolymph pathways. Based on our data, we then formulated a hypothesis suggesting that dissipation of energy for transporting hemolymph to the flight muscles could limit development of large-winged hawkmoths. These larger hawkmoths must address the need to maintain the required rate of fuel transport for flight by having thicker hemolymph enriched with the fuel carriers and, therefore, more muscles in the thorax, which would limit the permeability of flow.

METHODS

Selection of species

Hawkmoths are known for their vigorous flight and remarkable ability to hover, with wingbeat
frequencies up to 20-50 Hz[29,30]. This large range of wingbeat frequencies suggests that in
different hawkmoth species the hemolymph viscosity affecting its circulation is subject to
different constraints. Our evaluation of adult hemolymph viscosity is based on 12 species of
hawkmoths. We sampled at least five individuals per species (except Xylophanes tersa, which
had four individuals; Table S1). In addition to hawkmoths, the viscosities of two non-hovering
but long-distance flying butterflies, the Painted lady (Vanessa cardui) and Monarch (Danaus
plexippus) [31-33], were probed to provide more robustness to the method. In total, we
sampled the hemolymph of 78 individual hawkmoths and 23 individual butterflies (Table S1).
Eleven species of our hawkmoths with a long proboscis hover during feeding and are expected
to consume a significant amount of lipid during flight [14,25,32,34–36]. In contrast, Ceratomia
catalpae is a short-proboscis species of hawkmoth that does not hover over flowers. All of our
hawkmoths forage during the evening and night, except the diurnal Hemaris diffinis. Our taxon
sample includes some of the smallest species with the shortest wings (e.g., Paratrea plebeja)
and some of the biggest species with the longest wings (e.g., Manduca rustica) in eastern North
America[37].

Insect collection and rearing

Two hawkmoth species (*C. catalpae* and *Manduca sexta*) and both species of butterflies (*V. cardui* and *D. plexippus*) were reared in the laboratory, following our standard procedures[7]. We captured all other hawkmoths, using an aerial hand net, in the South Carolina Botanical Garden (Clemson University) from August to October 2021 and 2022. Field-collected

hawkmoths were refrigerated at 4 °C for at most two days before extracting their hemolymph. For butterflies and *M. sexta* reared in the lab, we fed them a sucrose solution (0.5 g/ml) at room temperature over a 2-week period and refrigerated them at 4 °C between feeding sessions. During this period, hemolymph viscosity did not change, indicating that the insects were not dehydrated (Fig. S1). Because adults of *C. catalpae* (putatively a non-feeding species) were not fed, we extracted their hemolymph within 2 days after emergence from the pupae.

Characterization of hemolymph viscosity

Hemolymph extraction and body measurements. For hemolymph extraction, the insects were restrained by the wings with a spring-type clothespin. A small incision was made in the membrane at the wing base, which provided a minimally disruptive exit for hemolymph. A 5- μ l or 20- μ l capillary tube (Drummond, 1-000-0050 or 3-000-210, respectively) was applied to the wound and the hemolymph collected by capillary action as it exited the body (Fig. S2). Once a meniscus formed, 0.5-3.0 μ l of hemolymph were collected from butterflies within 5 seconds to several minutes. The collected hemolymph volume for hawkmoths varied from 25 μ l to 130 μ l. Hemolymph inside the capillary tube did not change its colour and viscosity within the time of the experiment, suggesting that evaporation and oxidation were not significant. We also evaluated hemolymph viscosity within 20 minutes after collection, which indicated that no clotting occurred before 20 minutes (Fig. S3).

To measure body length and width, we photographed individuals of all species of hawkmoths before hemolymph extraction. We then measured body length as the distance between the distal end of the abdomen and the distal end of the head, and body width as the distance between the wing bases. Given that hawkmoths have an almost uniformly cylindrical body, we inferred their body volume as the volume of a circular cylinder, using body length

and width measurements. From the same images, we measured forewing length from the wing base to the outermost tip. We performed all measurements with ImageJ[38]. Measurements for *V. cardui* and *D. plexippus* were taken from the literature[39,40].

129

130

131

132

133

134

135

136

137

138

139

140

141

142

143

144

145

146

147

148

149

126

127

128

Magnetic rotational spectroscopy. To measure hemolymph viscosity, nickel nanorods of $d \sim 200nm - 400 nm$ diameter and $L_0 \sim 7 \mu m - 13 \mu m$ length, with remanent magnetization of $M_r = 224 \text{ kA/m}[41]$, were dispersed in methanol by sonication. A droplet of the nanorodmethanol suspension was placed on a glass slide and allowed to dry at 23 \pm 1 0 C and 50 \pm 20% humidity. Hemolymph was placed on the dried nanorod-methanol residue and stirred with a glass rod to disperse the nanorods. Pure nitrogen gas pre-bubbled through deionized water to saturate it with water vapor was passed through an environmental chamber[27] and over the surface of the sample. Water evaporation was significantly slowed, and no oxidation occurred, which was verified by the absence of colour change in the sample. In a series of additional experiments, the hemolymph droplets were directly exposed to air (21-23 °C). To eliminate any effects of the hemolymph-substrate and hemolymph-air interfaces on viscosity, only nanorods inside the drop (6 μm below the air-hemolymph interface and \sim 6 μm above the substrate) were used. The data show no influence of air on viscosity measurements within ~ 5 – 20 min (Fig. S3); therefore, to increase the processing time and minimize the effects of an immune cascade reaction on viscosity[7], the majority of experiments were performed on free droplets.

A rotating magnetic field of $B = 30 - 200 \,\mu$ T in amplitude and $\omega = 1 - 5 \,Hz$ in rotation frequency was applied to rotate the nanorods. This MRS methodology allowed us to probe rheological properties of hemolymph at the natural loads generated by insect locomotion and heart pumping. For example, a nickel nanorod 200 nm in diameter and 10 μ m in length in

water of $1 \, mPa \cdot s$ viscosity senses the torque on the order of $10^{-17} \, N \cdot m$. For comparison, the torque measured by standard plate-cone viscometers with a gap thickness of about 200 µm, is many orders of magnitude larger $(10^{-3} \, \text{N·m})$ (Viscometer manual available at: https://www.brookfieldengineering.com/products/rheometers/-/media/f8d571d827dc4efb8c097caf18ef11ae.ashx), confirming that the hemolymph constituents could be destroyed by using this instrument. Our measurements have high accuracy, as shown with an example of a $\sim 10 \, \mu L$ hemolymph droplet extracted from *M. sexta* (Fig. 1).

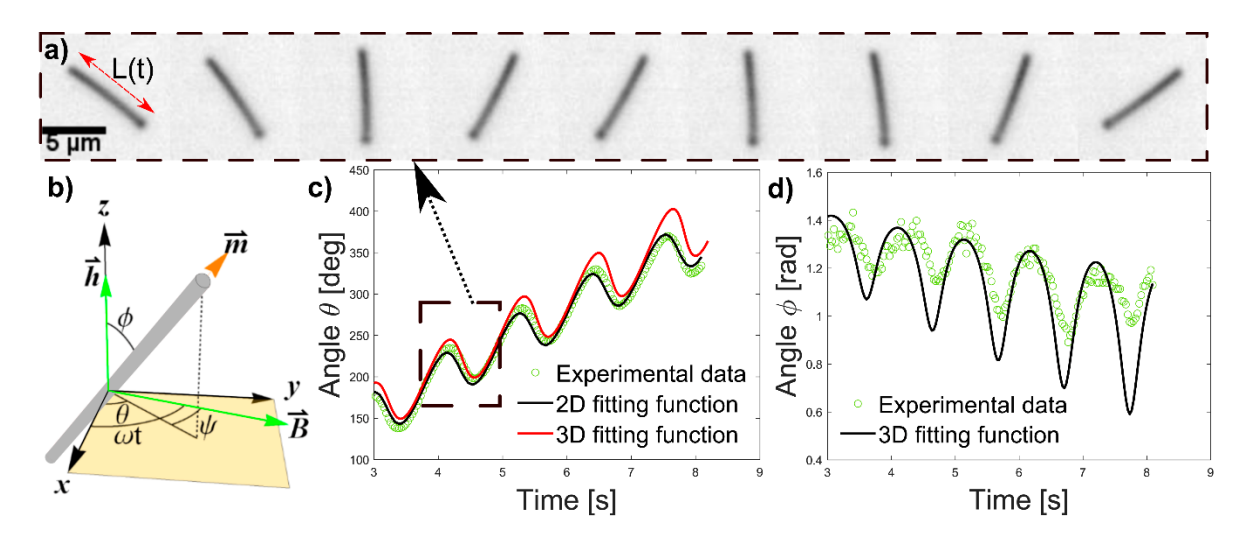


Figure 1. (a) Representative sequence of frames (~1 s) of a nanorod rotating inside hemolymph, following magnetic field changes. (b) Schematic of a nanorod (grey bar) orientation in a laboratory xyz system of coordinates. The angle θ is taken between the x-axis and the projection of the nanorod long axis onto the xy-plane; the angle ϕ is taken between the z-axis and the nanorod long axis, which is coincident with the magnetic moment $m = \pi d^2 L_0 \cdot M_r$. An auxiliary angle, $\psi = \omega t - \theta$, is introduced to describe the relative direction of xy projection of magnetic moment m with respect to the rotating field m. The actual physical length m0 of the nanorod-remains constant during 3D rotation, while the length m1 is the length of the nanorod projected onto a 2D plane at a given moment m2. m3 when the nanorod is not parallel to the 2D plane. To know the difference between these

measures, we calculated the angle ϕ by solving $\sin \phi(t) = L(t)/L_0$ for ϕ). (c) Example of 2D rotation data, $\phi = \pi/2$, where the nanorod angle θ is fitted with the model[42]. Green circles show the experimental data retrieved from the sample, the dark solid line shows a function fitted for 2D rotation, and the red line shows the line fitted through a function for 3D rotation. This set can be fitted with both 2D and 3D rotation functions because angle θ is projected on the xy plane. (d) The same data, but with the angle ϕ as the projection on the z axis. Thus, only 3D rotation function can be applied[28]. The parameters of the fitted lines in (c) and (d) were used to estimate hemolymph viscosity.

The rotation was recorded and the nanorod length and direction were analysed using Labview and MatLab algorithms that allowed us to track the nanorods and fit their trajectories, using the models of 2D and 3D rotations of nanorods[27,28]. Both 2D and 3D motions of nanorods were analysed, and a system of differential equations describing nanorod rotation[28] was numerically solved to extract the fitting parameter $\omega_c = \frac{\pi d^2 L_0 \cdot M_r \cdot B}{4\Gamma \cdot \eta}$, where η is the hemolymph viscosity and $\Gamma = \frac{\pi L_0^3}{3 \ln(L_0/d) - 2.4}$ is the nanorod form-factor.

We report only data collected over about 20 minutes when no change of relative viscosity was observed (Fig. S3). Viscosity remained constant for about 20 minutes, then rapidly increased, suggesting formation of clots or polymer aggregates[7]. This constant value of viscosity over a 20-minute time frame was interpreted as the viscosity of hemolymph in the insect body. The MRS calibration was performed by measuring viscosities of DI water and 30% glycerol solution at room temperature (23 °C) and comparing them with the reference values. The volume of hemolymph extracted from individual insects varied significantly. Thus, the number of nanorods used and the number of measurements for hemolymph droplets differed (Table S1).

To obtain hemolymph viscosity for a given droplet, we averaged the data for different nanorods in the same droplet. The average viscosity for an individual, thus, is the average viscosity of all the droplets tested, and the average viscosity for a species is the average of the viscosity of the individuals. We also used only the lowest measured values because nanorods with greater viscosity values could be either rotating near the droplet surface or substrate, aggregated in larger rod-like clusters, or embedded in a domain with a flake of tissue or hemocytes. All these processes can increase viscosity.

The structure of hemolymph pathways in the thorax of hawkmoths

To study the structure of intermuscle space through which hemolymph flows, we imaged one individual of each hawkmoth species in our sample using micro-computed tomography (micro-CT) imaging. The hawkmoths were frozen at -76 °C the day after they were collected. To minimize the dehydration effect, they were shipped overnight to North Dakota State University Electron Microscopy Core Lab in Fargo, North Dakota, for micro-CT scanning. Freezing of live tissue at -76 °C prevents dehydration and minimizes artifacts associated with chemical treatment of tissues and is thus a good procedure to maintain tissue structure [43–45]. The scanning was conducted within two days after receiving the specimens. Each sample was placed at the top of a Kapton 40 tube with the head protruding. A GE Phoenix v|tome| x s X-ray micro-CT equipped with a 180-kV high power nanofocus X-ray tube xs|180nf and a high-contrast GE DXR250RT flat panel detector was employed to collect the micro-CT images. One thousand projections of the sample at a voltage of 60 kV and a current of 240 µA were acquired using a molybdenum target. Detector timing was 1500 ms and total acquisition time was 1 hour and 40 minutes. Sample magnification was 55.22x with a voxel size of 2.4 µm. We reconstructed the acquired images into a volume data set, using GE datos|x 3D-computer

the distance between the two halves of the longitudinal muscle fibres at five equidistant points along the thorax of the moth (Fig. 2). We did not evaluate the gaps between dorsoventral muscle fibres because the resolution was insufficient to make reliable measurements. Therefore, we focused on the pore spaces of longitudinal muscle fibres to have robust and reliable measures. To visualize, segment, and measure areas of the thorax, we used Slicer 3D v. 5.0.3[46].

Statistical analyses

Power requirements during hovering flight are typically estimated using the momentum theory of helicopter aerodynamics. The only parameters necessary are forewing length and body mass/volume. We used these parameters to evaluate their correlation with hemolymph viscosity and used comparative phylogenetic methods to model the evolution of these traits. For a proper comparative framework, we analyzed only hawkmoth species and excluded butterflies. We used the available multigene, time-calibrated phylogeny of the Sphingidae[47] as our phylogeny. The phylogeny contains 202 taxa with 10 species used as outgroups; all the rest were members of the Sphingidae. The authors of Ref. [47] time-calibrated the molecular tree using the available fossil record at the time, and the origin of Sphingidae was estimated as ~50 Myr (HPD: 55-40 Myr). We pruned the tree to match the 12 hawkmoth species in our sample using the package *ape*[48]. Before proceeding with analysis, we visually inspected scatterplots of hemolymph viscosity and body volume, and hemolymph viscosity and proboscis length, to provide an unbiased first approximation of the data[49]. These inspections suggested that the relationships might not be linear. Thus, we also built models with a quadratic parameter.

We built the phylogenetic linear regressions using the package 'phylolm' in R v4.1.1 [50,51] separately for body volume and forewing length. We used average body volumes and average forewing lengths because the available package did not allow us to probe variations of the body volume and forewing length. In one set of analyses, we used hemolymph viscosity as our dependent variable, average body volume as our independent variable, and phylogeny as our variance-covariance matrix[52]. In another set of analyses, we used hemolymph viscosity as our dependent variable, average forewing length as our independent variable, and phylogeny as our variance-covariance matrix. We also added the error associated with hemolymph viscosity measurements to the variance covariance of the model, as described in [50]. Lastly, we tested which evolutionary regimes best fit the models by fitting three different evolutionary regimes to the models: Brownian motion (BM), a single optimum Ornstein-Uhlenbeck (OU) model with an ancestral state estimated at the root (OUfixedRoot), and another lambda model (lambda).

To handle the different possibilities of model building (e.g., linear or quadratic parameters, evolutionary models), we adopted a stepwise rationale. In the first step, we tested which evolutionary model fitted our data best. To do so, we built the most complex models (i.e., with the quadratic parameter) and ran it with the three evolutionary models. We then used Akaike's Information Criterion (AIC) to select the best-fit model for each predictor. Models with Δ AIC > 2 were considered poorly fit, and we used the model with the lowest AIC. When models differed by no more than two units of AIC, we used those with the lowest number of parameters as the best-fit models[53]. In the second step, we used the 'phylostep' function in the *phylolm* package to do a stepwise selection in both directions. This algorithm starts from the most complex model and decreases complexity while also doing the opposite: the algorithm fitted the simplest model and added complexity. The 'phylostep' function compares the AIC of the model with more parameters against the model with less parameters. Once the difference

between the models becomes higher than 2 AIC units, the stepwise selection stops. When the best solution is found, and when the solution from both directions matches, we have the bestfit model. We used a bootstrap method with 10,000 replicates to calculate the confidence interval of the parameters estimated on the best-fit model. If the confidence interval of the parameters did not overlap zero, we considered that parameter to be significant. To evaluate the influence of the largest species, M. rustica, on the results, we ran two additional sensitivity analyses. First, we used raw data on hemolymph viscosity and forewing length and fitted these data using the Excel "trendline" polynomial fit with and without *M. rustica*. Since the parabolic dependence was still a good fit (based on Chi-square goodness of fit tests, see Supplementary Material), we also excluded the second largest species, M. quinquemaculata, from the sample. With the two largest species, the linear fit appears to be the best. This analysis suggested that M. rustica is not an outlier and the two largest moths force the curve to bend. Second, we considered phylogenetic correlations between species. We removed *M. rustica* from our sample and ran the same phylogenetic model. Then, we compared the best fit to the data with and without M. rustica, using goodness of fit metrics (e.g., R2, sum of squares). This method confirmed a similar pattern that emerged from the first sensitivity analysis. The details of these analyses and the results are described in Supplementary material (section "Sensitivity analyses").

283

284

285

286

287

288

265

266

267

268

269

270

271

272

273

274

275

276

277

278

279

280

281

282

RESULTS

Hemolymph is a Newtonian fluid more viscous than water

Analyses of the viscous drag on nanorods exerted by hemolymph of adult Lepidoptera, with its small concentration of hemocytes, indicate that the hemolymph behaves as a Newtonian fluid with constant viscosity [7,27,28,42,54]. Hemolymph viscosity of all butterflies and hawkmoths

varied in the range $1.3 \pm 0.25 \, mPa * s < \eta < 2.2 \pm 0.5 \, mPa * s$ and was always greater than that of DI water, $\eta = 0.9 \pm 0.1 \, mPa * s$ (Table S1). The twofold greater viscosity with respect to water raises the question of what causes enhanced viscous dissipation of energy in insects, especially during prolonged flight. Given that viscous dissipation is important for the total energy budget, we evaluated the correlation of viscosity with additional morphological parameters influencing the energy budget in our hawkmoths.

Internal structure of the thorax and mechanisms of hemolymph circulation

Fuel comes from the fat body in the abdomenand is guided to the flight muscles by the dorsal vessel. When hemolymph exits the anterior portion of the dorsal vessel (i.e., aorta) and flushes toward the head, it preferentially moves backward to the abdomen [55]. In the reverse pumping [55], the hemolymph flows from thorax to aorta and back to the abdomen. The estimates given in Supplementary material for small and large resting hawkmoths suggest that the cardiac flow through thoraxes is mostly controlled by inertial forces. In resting hawkmoths, the flight muscles are not activated, i.e. the intermuscle distances remain unchanged.

In hovering hawkmoths, the heartbeat frequency increases[56,57] and the thoracic contractions help to propel the hemolymph (Fig. 2c, d). The internal thorax is composed mainly of two sets of muscles. The longitudinal flight muscles, which contract to move the wings down, and the dorsoventral muscles, which contract to move the wings up (Fig. 2). In the upstroke, hemolymph is forced into intermuscle pores and in the downstroke it is squeezed out from these pores. Again, the flow direction is dictated by the permeability gradient: the less permeable head resists the flow and hence hemolymph moves preferentially toward the abdomen [55]. Thus, against the background of unidirectional circulatory flow, these contractions increase the flow through the porous thorax.

All analyzed species presented the same overall conformation inside, the main difference being the spaces (pores) between muscle fibers. Intermuscle pores in small hawkmoths were somewhat wider (Fig. 2, S4 and Table S3) than in large hawkmoths. For instance, *Manduca rustica* (Fig. 2a,e,f,g), a large hawkmoth, had little space between muscle fibers. The maximum distance between the longitudinal muscle fibers for this species was $h_{max} = 0.09$ mm, whereas the average distance between muscle fibers along the body axis was $h_{av} = 0.08$ mm (± 0.009 mm). The smaller *Paratrea plebeja* (Fig. 2b,h,i,j), on the other hand, had more space between muscle fibers, which greatly increased the size of the pores through which hemolymph could flow. The maximum distance between the longitudinal muscle fibers of this species was $h_{max} = 0.4$ mm, whereas the average distance between muscle fibers along the body axis was $h_{av} = 0.25$ mm (± 0.07 mm). Thus, both species had similar pore structure in their thoraxes, but the amount of space for hemolymph to flow through differed between species. These pores represent the hemolymph pathways and, hence, their sizes provide insight into the flow constraints and associated hemodynamic mechanisms of the energy dissipation. The pore spaces for all the species can be found in Fig. S4 and Table S3.

The Reynolds number, Re, is an important parameter showing whether the hemolymph inertia or viscous drag is a prevailing factor in the flow[58]. For the intermuscle pathways, one can estimate the Reynolds number as $Re = \rho \cdot v \cdot h_{av}/\eta$, where $\rho \approx 1000 \, kg/m^3$ is the hemolymph density and v is its velocity. We need to distinguish the hemolymph flow caused by the heart pumping from the flow caused by contraction and expansion of the intermuscle pores.

When the intermuscle pore sizes change due to muscle contraction, the regime of cardiac flow changes as well. Without measurements, the estimate of the Reynolds number for cardiac flow is difficult to provide as some pores could be completely collapsed, thus blocking

the flow at that moment. Given the background of forced cardiac flow, hawkmoths can develop pulsatile flow by muscle contraction. This flow can be evaluated as follows.

The heartbeat frequency f_{heart} in hawkmoths is at least one order of magnitude smaller than the wingbeat frequency f[30,55]: in the thorax, the insect could push its hemolymph in and out ~ 20 times during one stroke of its dorsal vessel (heart). The upper estimate of hemolymph velocity during muscle contraction is estimated as the rate of shutting off the intermuscle pores, $v \sim f h_{av}$; accordingly, $Re = \rho \cdot f \cdot h^2_{av}/\eta$. Taking as the wingbeat frequency $f = 20 \, Hz$ and data for viscosity from Table S1, we have Re = 0.8 for *Paratrea plebeja* and Re = 0.09 for *Manduca rustica*. For small hawkmoths with wingbeat frequency greater than 20 Hz, but the same pore dimensions, the Reynolds number may be somewhat greater than 1.

Thus, for pulsatile flow at $Re \sim 1$, inertial flow of hemolymph through intermuscle pathways could be an important transport mechanism for fuel delivery to the flight muscles in small-winged hawkmoths. At Re < 1, the hemolymph pulsatile flow is mostly controlled by viscous drag and, hence, the mechanism of fuel delivery to the flight muscles in large-winged hawkmoths is different.

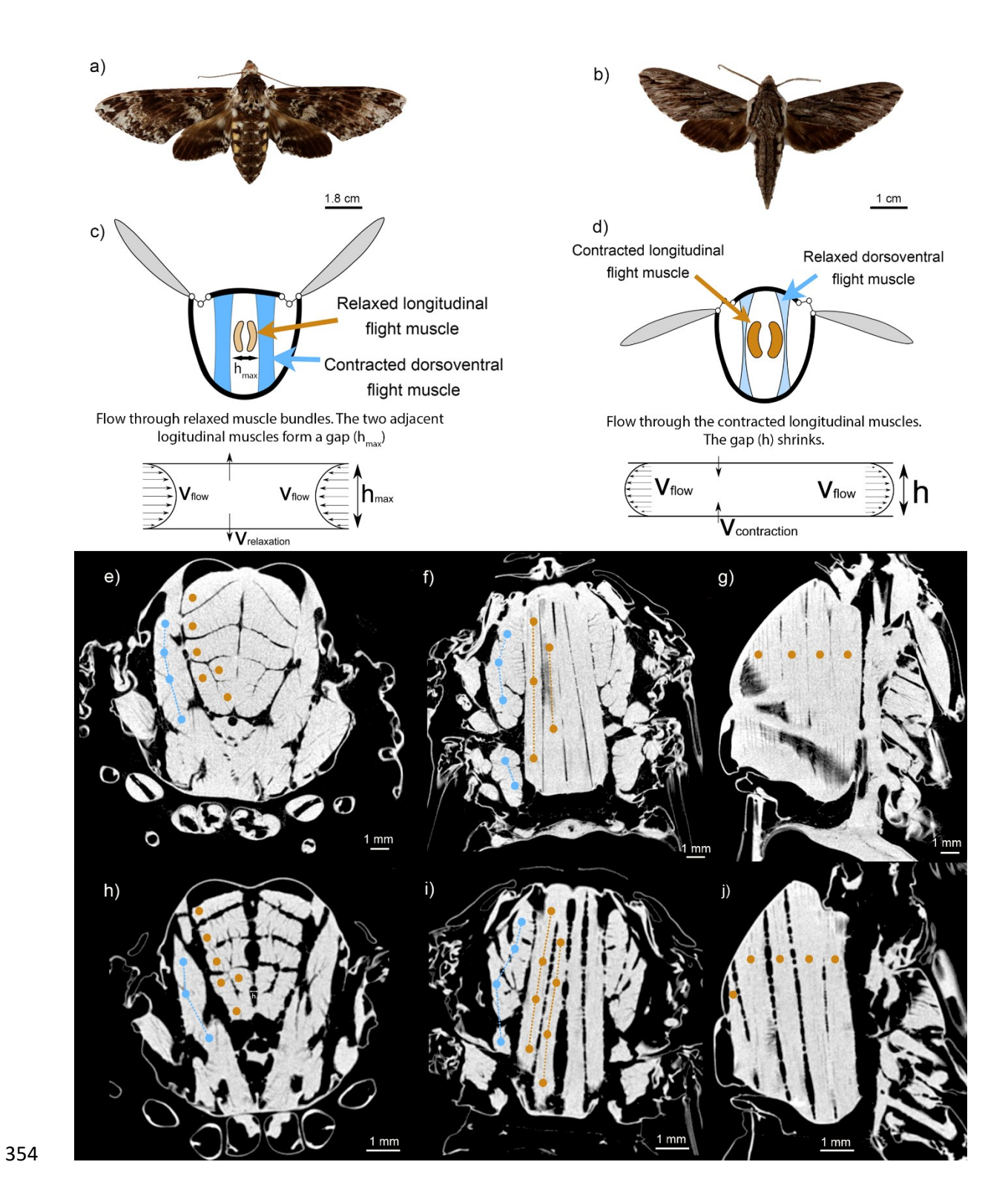


Fig. 2. (a) Manduca rustica and (b) Paratrea plebeja. (c) and (d) Schematic representations of the flight muscle movement, exoskeleton deformation, and hemolymph flow between intermuscle spaces. In (c), the longitudinal muscles are relaxed and the dorsoventral flight muscles are contracted, pulling the thoracic tergum (dorsum) and sternum (venter) closer

together and causing the wings to move upward. In (d), the dorsoventral muscles are relaxed while the longitudinal muscles are contracted, pulling the anterior and posterior portions of the thorax closer together and causing the wings to move downward (e)-(g). Different sections of the thorax of *M. rustica*. (e) is a cross-section, (f) is a longitudinal section (dorsal view), and (g) is a dorsoventral section (lateral view). Blue dots denote the dorsoventral flight muscles. Thus, one muscle bundle can contain several dots, which are connected using dashed lines. For instance, in (e) the three blue dots show the same muscle bundle connecting the tergum to the sternum. In (f), all bundles of the dorsoventral flight muscles can be seen, whereas in (g), the dorsoventral muscles cannot be seen. Because the muscles are axially symmetric, only one side of the moth is marked with dots. Golden dots denote the longitudinal flight muscles. In (h), (i), and (j) the sections are in the same orientations as (e), (f), and (g), respectively, but are of *P. plebeja*, which has more space between the muscle bundles. In (h), the space between the muscles is denoted with the letter h.

Does hemolymph viscosity correlate with body volume or forewing length in hawkmoths?

The Brownian evolutionary model provided the best fit among all models, regardless of whether we correlated viscosity with the body volume or forewing length (Table S3). The stepwise analysis showed that hemolymph viscosity was not correlated with body volume in hawkmoths (Fig. 3a). The best model contained only the intercept (Table 1a). However, hemolymph viscosity was associated quadratically with average forewing length (Fig. 3b, Table 1b). Thus, species with short and long forewings had less viscous hemolymph when compared to species with medium-length forewings (Table 1b). The confidence intervals estimated for both linear and quadratic parameters did not encompass zero (linear: 1.338 [95% CI: 0.363, 2.333], quadratic: -0.15 [95% CI: -0.265, -0.036], adjusted r-squared: 0.25). When

the data were analyzed without phylogeny, parabolic viscosity dependence was the best least-square fit for the whole dataset and the dataset with removed *M. rustica*. Linear dependence was the best least-square fit only without *M. rustica* and *M. quinquemaculata* (Fig. S5). When the phylogenetic correlations were included, the linear fit and a quadratic fit were indistinguishable from each other based on their AIC and degrees of freedom (Table S4). However, the linear approximation of viscosity versus mean forewing length had a worse fit to the data when compared with the quadratic approximation (Fig. S5, Table S5). Thus, all analyses yielded the quadratic approximation with a well-developed maximum as the best fit.

Members of the hawkmoth subfamily Macroglossinae had medium values of viscosity, whereas those of the subfamily Sphinginae had a wider range of viscosity (Figure 3c, d). The ancestral character reconstruction, performed using the function 'contMap' with the 'phytools' package [59] reinforced that pattern. Given that the Sphinginae had shorter branch lengths, hemolymph viscosity changed more rapidly between sister taxa (e.g., *C. catalpae* and *P. plebeja*), whereas the Macroglossinae had longer branches and the changes in viscosity were not as fast or as pronounced as in the Sphinginae.

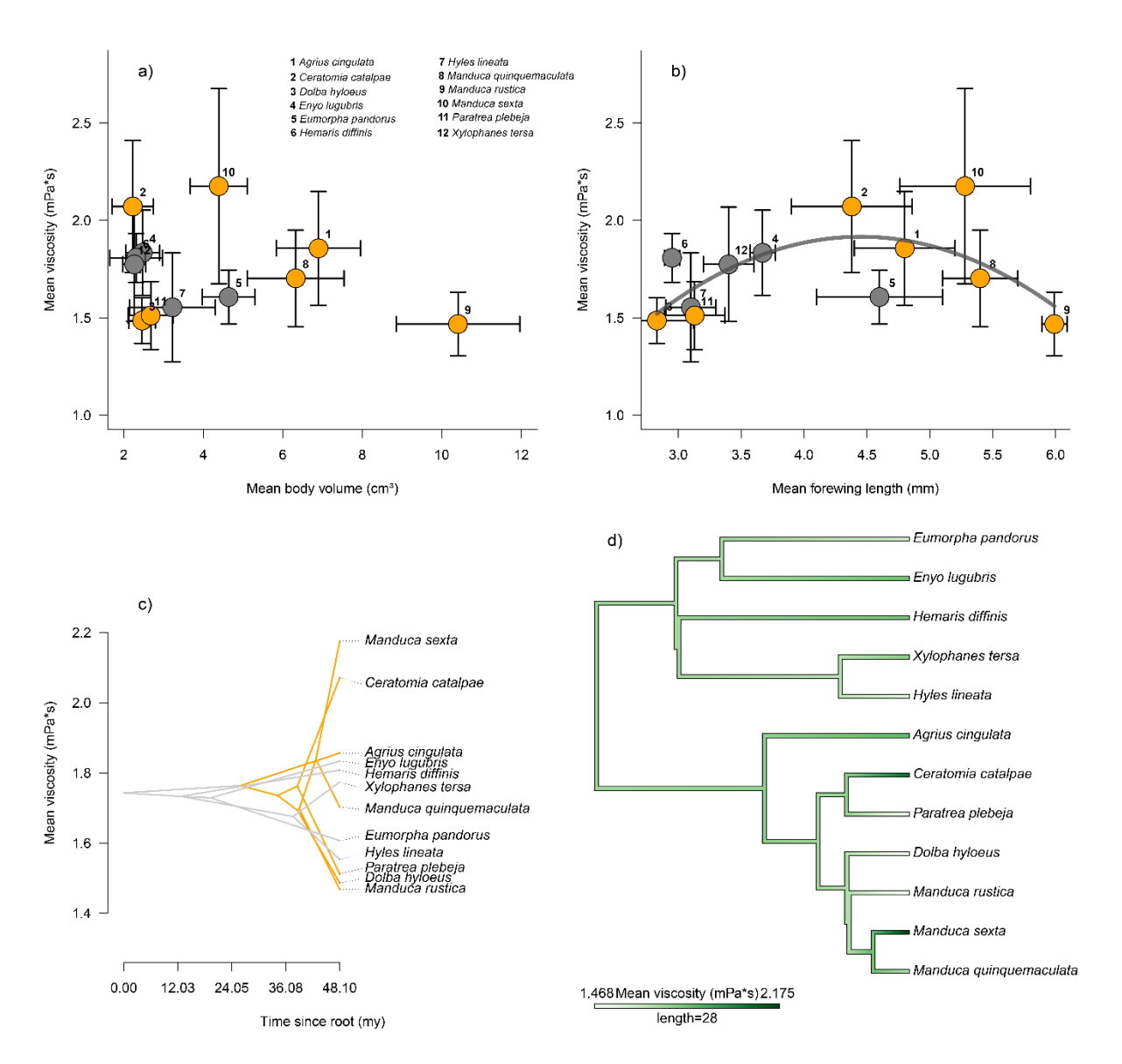


Fig. 3. Body volume (a) has no correlation with hemolymph viscosity, but forewing length (b) has a quadratic association. Each dot represents a species, and the line represents the best-fit line estimated with phylogenetic linear regression. Orange dots represent species of the family Sphinginae, and gray dots represent species of the family Macroglossinae. Whiskers represent the standard deviation of the samples accounted for in the model. (c) A phenotypic diagram with the phylogeny distorted to accompany changes in the mean phenotype (hemolymph viscosity). Orange lines denote the subfamily Sphinginae, whereas gray lines denote the subfamily Macroglossinae. (d) Ancestral reconstruction of hemolymph viscosity. Values along

the branches of the phylogeny were calculated using the 'contMap' function of phytools package in R [59]. We also used this phylogeny to model trait evolution in (a) and (b).

Table 1. Regressions between hemolymph viscosity and (a) body volume and (b) forewing length, using different evolutionary models. We built full models (i.e., with all the parameters) and used stepwise selection to find the best model. When $\Delta AIC > 2$, the model was considered a poor fit. If models tied with the same AIC value, we chose the model that added the fewest parameters (fewest degrees of freedom, DF) to the data. Forewing length does not have an 'intercept only' model because the full model was better fitted than the others it was compared with in the first round. Thus, no 'intercept only' model was needed to find the best solution.

MODEL	AIC	ΔΑΙΟ	DF
(a) Body volume			
Intercept only	3.52883	-	3
Intercept + quadratic relationship	4.53113	1.00	4
Intercept + linear relationship	4.87439	1.34	4
Intercept + linear + quadratic relationship	5.88718	2.35	5
(b) Forewing length			
Intercept + linear + quadratic relationship	1.59344	-	5
Intercept + linear relationship	4.83302	3.23	4
Intercept + quadratic relationship	5.12366	3.53	4

DISCUSSION

Physico-chemical regulators of hemolymph viscosity in hawkmoths

Aerodynamic requirements and physiological constraints

While hovering[60–62], a hawkmoth uncoils its proboscis, tethers itself to a flower, and is able to fully balance its weight by the lift force generated by the flapping wings. With each flap, the

thorax deforms and moves hemolymph through the body. The thorax is densely packed with flight muscles[31,32]; thus, from a materials point of view, the thorax is a porous body. The mean flow velocity through a slit-like pore of opening h_{av} is proportional to the pore opening squared, h_{av}^2 , and inversely proportional to hemolymph viscosity[58]. Therefore, the denser the muscle pack, the smaller the pore opening, and the stronger the pressure gradient needed to move hemolymph through the thorax[10]. And the greater the hemolymph viscosity, the greater the required pressure gradient.

Heavy hawkmoths must produce greater lift, and therefore, aerodynamically need larger wings, which they flap less vigorously[30,63,64]. In contrast, lighter hawkmoths must flap their wings faster to generate the lift needed to support their body[30,63,64]. Larger hawkmoths, with their smaller pores in the thorax and larger body volume and wingspan, must circulate hemolymph over a longer, more tortuous pathway through the intermuscle pores to the abdomen and back to provide fuel to the muscles and remove waste. Smaller hawkmoths must move hemolymph faster to refresh their more rapidly contracting muscles with new fuel and remove the waste. Cardiac pulses establish a background hemolymph flow while the flight muscle contractions generate pulsatile flow on this background. Intermuscle pores in small hawkmoths are somewhat wider and the Reynolds numbers for pulsatile flow may be of the order of 1, suggesting a different inertial flow mechanism of fuel transport. Low viscosity supports both inertial cardiac flow and pulsatile flow of hemolymph through the thorax in small-winged hawkmoths with large pore openings and a viscosity-controlled pulsatile flow mechanism in small-winged and large-winged hawkmoths with smaller pore openings.

Metabolic requirements may conflict with functioning of hemolymph biopolymers and dehydration

For efficient combustion of fuel during flight, the flight muscles of insects must maintain high temperature [15]. For example, the hemolymph temperature of M. sexta increases to more than 40°C during flight[15]. Viscosity of freshwater decreases with increasing temperature; for example, at 10°C , viscosity of water is $1.31 \, mPa \cdot s$ and at 40°C it drops to $0.65 \, mPa \cdot s$. Aqueous salt solutions are slightly more viscous than freshwater, but the change of their viscosity follows the same pattern. Therefore, when the temperature of the flight muscles increases, the circulating hemolymph, consisting of 90% water, is expected to warm up and decrease its viscosity. As the velocity of hemolymph moving through the intermuscle pores is inversely proportional to viscosity, this temperature rise would result in greater velocity at the same pressure gradient. Therefore, the heat works in favour of the hovering moths: it decreases its viscous dissipation.

During prolonged flight, hawkmoths are able to regulate their thoracic temperature, maintaining it at a certain level, above which the moths cannot fly[15]. This critical temperature increases with moth mass[15,64]. Thus, large moths producing large lift decrease their hemolymph viscosity by raising the thoracic temperature, but then require more fuel and hence more lipoprotein shuttles. Having a lower viscosity at room temperature would benefit the moth during flight. Indeed, when more lipoprotein shuttles are generated, the associated increase of their viscous drag at the lower base viscosity might not be particularly critical.

Thus, flying insects that rely on lipid fuel have to solve the physiological dilemma of increasing the concentration of lipoproteins associated with shuttling lipid fuel from the fat body to the flight muscles while decreasing the viscous dissipation associated with hemolymph circulation through the body. This paradox is the main challenge for decreasing the cost of the energetics of prolonged flight. Heinrich hypothesized that the thoracic temperature of large hawkmoths cannot increase above a lethal threshold of 45 °C[15, 59]. This temperature could be associated with denaturation of some biopolymers that circulate in the hemolymph or are

present in the tissue. Data on thermophysical properties of hemolymph and tissue are not available, and this hypothesis remains untested. Furthermore, viscosity of flying hawkmoths cannot be directly measured with our technique, and we can only suggest that it would be comparable to the viscosity of small flying hawkmoths, as the data on the room-temperature analysis suggest.

For hovering moths, convective heat and mass transport are of great importance [65,66]. Therefore, the rise of thoracic temperature could significantly increase the evaporation rate of water, potentially leading to dehydration. With water evaporating, but the demand of fuel remaining the same, the concentration of lipoprotein shuttles increases and the hemolymph is expected to become more viscous. This constraint also might influence the demand on temperature regulation, allowing the insect to conserve water and ensuring that increased hemolymph viscosity from evaporative water loss would not imperil the insect.

Evolutionary perspectives

Hawkmoth phylogeny informs viscosity—size relationships

The variation in hemolymph viscosity differs between the subfamilies Macroglossinae (e.g., *Eumorpha*) and Sphinginae (e.g., *Manduca*). The Macroglossinae possess medium hemolymph viscosities, whereas the Sphinginae include a wide range of viscosity values. Although these subfamilies demonstrate robust monophyly, small differences and apomorphies are not trivial[67,68]. Ecologically, the subfamilies are similar, such as in their use of plant types, long proboscises for acquiring nectar, and the ability to produce sounds to jam bat radar[47,69]. The range of forewing length, however, differs: the Sphinginae have wider variation of forewing length than do the Macroglossinae. Although our sample of Macroglossinae species includes short to medium-length forewings and medium hemolymph viscosities, our sample of

Sphinginae species covers the entire spectrum of forewing lengths (Fig. 3b). The broad range of hemolymph viscosity in Sphinginae, tied to the range of forewing sizes, suggests that viscosity is tied to the load the animal faces during flight. The third of the three subfamilies of hawkmoths, the Smerinthinae, consists mostly of weaker fliers that neither hover nor feed from flowers, except members of the tribe Ambulycini. Therefore, the Smerinthinae aerodynamics would not necessarily limit hemolymph circulation and, hence, their hemolymph viscosity would not be constrained as much by their body and wing sizes.

Hemolymph viscosity and the evolution of insect flight

The internal circulating milieu is well-studied in the physiology of insects[11], but its physical properties are typically not considered in the evolution of insect flight or size transformations, either toward gigantism or miniaturization. Yet, as we have shown, hemolymph viscosity imposes constraints on flight dynamics, particularly in relation to wing size. Given that forewing length can influence flight energetics, the evolution of wings and flight should be correlated with the evolution of hemolymph viscosity. Differences in the metabolic demands of flight are probably related to the different strategies for modulating hemolymph viscosity.

Accordingly, hemolymph viscosity should track the evolution of insect flight from its origins. Although an isometric change in body size might be an evolutionary mechanism for generating functional change in a structure[70], in the case of wings for flapping flight, the change at some point would require concomitant adjustments of hemolymph viscosity. The most dramatic modifications of hemolymph viscosity would be expected in hovering insects (e.g., hawkmoths and syrphid flies) and rapidly flying insects (e.g., blow flies, honey bees, and bot flies). The fine-tuning of viscosity might be especially acute for diurnal insects operating in full sunlight, which need to account not only for intrinsic heat production, but also for

external heat in maintaining their water balance and, in tandem, their hemolymph viscosity.

Thus, hemolymph viscosities within and among species might also be sensitive to latitudinal and elevation gradients as well as changes in climate.

Hemolymph characteristics associated with metamorphosis reflect responses to different selection pressures. The hawkmoth *M. sexta*, for instance, experiences a marked reduction in hemocyte numbers from larva to adult[6,7], beginning in the final-instar larva[71]. Larvae experience intense selection pressure from wounding by parasitoids and predators and from ingested pathogens, and the immune response is mediated by hemocytes[72]. As assaults from parasitoids and pathogens decrease in the adult stage, hemocyte counts could be lowered to accommodate the selection forces driving efficient hemolymph circulation, including its viscous nature, during sustained or vigorous flight.

CONCLUSIONS

Comparative analysis of hemolymph viscosity in adult hawkmoths revealed a new physiological paradox regarding energetic costs of flying insects and established a reference for future studies. Although the lack of biochemical data on small amounts of hemolymph from individual hawkmoths prevents predictive modelling of physiological flows, we were able to show that viscosity of hawkmoth hemolymph is correlated with wing size in a quadratic, rather than linear, pattern. The analysis demonstrated that small-winged hawkmoths with a high wingbeat frequency and large-winged hawkmoths with a slower wingbeat frequency but greater lift both have viscosities approaching that of water. The hawkmoths with mid-sized wings have moderate wingbeat frequencies and wing sizes that would allow greater hemolymph viscosity. Overall, we showed that the metabolic demands of flight correlate with significant changes in circulatory strategies via modulation of hemolymph viscosity. Our

- analysis of the viscosity of two long-distance flying butterflies suggests that the tendency of
- hemolymph viscosity to increase with respect to that of water is an expected feature for
- 546 intensively flying insects.
- 547 Acknowledgements. We thank Jayma Moore and North Dakota State University Electron
- 548 Microscopy Core Lab in Fargo, North Dakota, for micro-CT scanning of hawkmoths.
- 549 Funding. This work was partially supported by NSF grant IOS 2014664 and the SC
- 550 EPSCoR/IDeA Program under NSF Award No. OIA-1655740. The views, perspectives, and
- content do not necessarily represent the official views of the SC EPSCoR/IDeA Program nor
- those of the NSF. The work of PHA was also partially supported by the NIFA/USDA, under
- project number SC-1700527, with Technical Contribution No. 7044 of the Clemson University
- 554 Experiment Station.
- Authors' contributions. Conceptualization: K.G.K.; experiments and data curation: A.B.,
- A.V.P., P.A., C.E.B.; visualization: A.B. and P.A.; phylogeny analysis: A.V.P. and P.H.A.;
- funding acquisition: K.G.K. and P.H.A.; project administration: K.G.K.; supervision: K.G.K.;
- writing original draft: K.G.K.; writing review & editing: K.G.K., P.H.A., A.B., A.V.P.
- **Declaration of interests.** The authors declare no competing interests.
- Data availability. Data and code are available at https://github.com/alexandrepalaoro/hemo-
- 561 viscosity

562

563 REFERENCES

- 1. Wigglesworth SVB. 1972 *The Life of Insects*. Weidenfeld and Nicolson.
- 565 2. Wigglesworth SVB. 1972 *The Principles of Insect Physiology*. Springer Dordrecht.
- 3. Nation JL. 2022 *Insect Physiology and Biochemistry*. 4th edn. Boca Raton: CRC Press. (doi:10.1201/9781003279822)
- 4. Li D, Scherfer C, Korayem AM, Zhao Z, Schmidt O, Theopold U. 2002 Insect
- hemolymph clotting: evidence for interaction between the coagulation system and the
- prophenoloxidase activating cascade. *Insect Biochemistry and Molecular Biology* **32**,
- 571 919–928. (doi:10.1016/S0965-1748(02)00030-9)
- 572 5. Scherfer C, Karlsson C, Loseva O, Bidla G, Goto A, Havemann J, Dushay MS, Theopold
- 573 U. 2004 Isolation and characterization of hemolymph clotting factors in *Drosophila*
- *melanogaster* by a pullout method. *Current Biology* **14**, 625–629.
- 575 (doi:10.1016/j.cub.2004.03.030)
- 6. Kenny MC, Giarra MN, Granata E, Socha JJ. 2018 How temperature influences the
- viscosity of hornworm hemolymph. *Journal of Experimental Biology* **221**, jeb186338.
- 578 (doi:10.1242/jeb.186338)

- 7. Aprelev P, Bruce TF, Beard CE, Adler PH, Kornev KG. 2019 Nucleation and formation of a primary clot in insect blood. *Sci Rep* **9**, 3451. (doi:10.1038/s41598-019-40129-0)
- 8. Brehélin M, editor. 1986 *Immunity in Invertebrates*. Berlin: Springer-Verlag. See https://link.springer.com/book/10.1007/978-3-642-70768-1.
- 9. Kinsey ST, Locke BR, Dillaman RM. 2011 Molecules in motion: influences of diffusion on metabolic structure and function in skeletal muscle. *Journal of Experimental Biology* **214**, 263–274. (doi:10.1242/jeb.047985)
- Malingen SA, Hood K, Lauga E, Hosoi A, Daniel TL. 2021 Fluid flow in the sarcomere.
 Archives of Biochemistry and Biophysics 706, 108923. (doi:10.1016/j.abb.2021.108923)
- 11. Pass G. 2018 Beyond aerodynamics: The critical roles of the circulatory and tracheal systems in maintaining insect wing functionality. *Arthropod Structure & Development* 47, 391–407. (doi:10.1016/j.asd.2018.05.004)
- 591 12. Hillyer JF, Pass G. 2020 The insect circulatory system: Structure, function, and 592 evolution. *Annual Review of Entomology* **65**, 121–143. (doi:10.1146/annurev-ento-593 011019-025003)
- 13. Kammer AE, Heinrich B. 1978 Insect Flight Metabolism. In *Advances in Insect* Physiology (eds JE Treherne, MJ Berridge, VB Wigglesworth), pp. 133–228. Academic
 Press. (doi:10.1016/S0065-2806(08)60266-0)
- 14. Casey TM. 1981 Insect Flight Energetics. In Locomotion and Energetics in Arthropods
 (eds CF Herreid, CR Fourtner), pp. 419–452. Boston, MA: Springer US.
 (doi:10.1007/978-1-4684-4064-5 16)
- Heinrich B. 2013 The Hot-Blooded Insects: Strategies and Mechanisms of
 Thermoregulation. Springer Science & Business Media.
- 16. Haruo C, Satoru M, Keiji H. 1969 Diglyceride-carrying lipoproteins in insect hemolymph
 isolation, purification and properties. *Biochimica et Biophysica Acta (BBA) Lipids and Lipid Metabolism* 176, 1–26. (doi:10.1016/0005-2760(69)90068-X)
- 17. Van der Horst DJ, Ryan RO. 2012 Lipid Transport. In *Insect Molecular Biology and Biochemistry* (ed LI Gilbert), pp. 317–345. San Diego: Academic Press.
 (doi:10.1016/B978-0-12-384747-8.10009-1)
- 18. Van der Horst DJ, Van Hoof D, Van Marrewijk WJA, Rodenburg KW. 2002 Alternative
 lipid mobilization: The insect shuttle system. *Mol Cell Biochem* 239, 113–119.
 (doi:10.1023/A:1020541010547)
- 19. Arrese EL, Soulages JL. 2010 Insect fat body: Energy, metabolism, and regulation.
 Annual Review of Entomology 55, 207–225. (doi:10.1146/annurev-ento-112408-085356)
- 20. Ryan RO, van der Horst DJ. 2000 Lipid transport biochemistry and its role in energy production. *Annual Review of Entomology* **45**, 233–260. (doi:10.1146/annurev.ento.45.1.233)

- 21. Gilbert LI, Chino H. 1974 Transport of lipids in insects. *Journal of Lipid Research* 15, 439–456. (doi:10.1016/S0022-2275(20)36764-X)
- 618 22. Mullins DE. 2013 Chemistry and Physiology of the Hemolymph. In *Integument*,
- Respiration and Circulation (eds GA Kerkut, LI Gilbert), pp. 355–400. Oxford, UK:
- 620 Pergamon Press.
- 23. Larson RG. 1999 *The Structure and Rheology of Complex Fluids*. Oxford, New York:
- Oxford University Press.
- 623 24. Dallmann SH, Herman WS. 1978 Hormonal regulation of hemolymph lipid concentration
- in the Monarch butterfly, Danaus plexippus. General and Comparative Endocrinology
- **36**, 142–150. (doi:10.1016/0016-6480(78)90059-X)
- Ziegler R, Schulz M. 1986 Regulation of lipid metabolism during flight in *Manduca sexta*. *Journal of Insect Physiology* 32, 903–908. (doi:10.1016/0022-1910(86)90106-X)
- 26. Pass G. 2000 Accessory Pulsatile organs: Evolutionary innovations in insects. *Annual Review of Entomology* 45, 495–518. (doi:10.1146/annurev.ento.45.1.495)
- 630 27. Aprelev P, McKinney B, Walls C, Kornev KG. 2017 Magnetic stage with environmental
- control for optical microscopy and high-speed nano- and microrheology. *Physics of*
- *Fluids* **29**, 072001. (doi:10.1063/1.4989548)
- 28. Palkar V, Aprelev P, Salamatin A, Brasovs A, Kuksenok O, Kornev KG. 2019 Rotating
- magnetic nanorods detect minute fluctuations of magnetic field. *Phys. Rev. E* **100**.
- 635 051101. (doi:10.1103/PhysRevE.100.051101)
- 636 29. Willmott AP, Ellington CP. 1997 The mechanics of flight in the hawkmoth *Manduca*
- 637 sexta. I. Kinematics of hovering and forward flight. Journal of Experimental Biology 200,
- 638 2705–2722. (doi:10.1242/jeb.200.21.2705)
- 30. Henningsson P, Bomphrey RJ. 2013 Span efficiency in hawkmoths. *Journal of The Royal Society Interface* 10, 20130099. (doi:10.1098/rsif.2013.0099)
- 31. Brown JJ, Chippendale GM. 1974 Migration of the monarch butterfly, *Danaus plexippus*:
- Energy sources. *Journal of Insect Physiology* **20**, 1117–1130. (doi:10.1016/0022-
- 643 1910(74)90218-2)
- 32. Masters AR, Malcolm SB, Brower LP. 1988 Monarch butterfly (*Danaus Plexippus*)
- thermoregulatory behavior and adaptations for overwintering in Mexico. *Ecology* **69**,
- 646 458–467. (doi:10.2307/1940444)
- 33. Talavera G, Bataille C, Benyamini D, Gascoigne-Pees M, Vila R. 2018 Round-trip across
- the Sahara: Afrotropical Painted Lady butterflies recolonize the Mediterranean in early
- spring. *Biology Letters* **14**, 20180274. (doi:10.1098/rsbl.2018.0274)
- 650 34. Nesbit RL, Hill JK, Woiwod IP, Sivell D, Bensusan KJ, Chapman JW. 2009 Seasonally
- adaptive migratory headings mediated by a sun compass in the painted lady butterfly,
- Vanessa cardui. Animal Behaviour 78, 1119–1125. (doi:10.1016/j.anbehav.2009.07.039)

- 35. Chapman JW, Reynolds DR, Wilson K. 2015 Long-range seasonal migration in insects:
- mechanisms, evolutionary drivers and ecological consequences. *Ecology Letters* **18**, 287–
- 655 302. (doi:10.1111/ele.12407)
- 656 36. David L, Zilli A. 2019 Moths: A Complete Guide to Biology and Behavior. Soho Press.
- 37. Hodges RW. 1971 The Moths of America North of Mexico. Fascicle 21. Sphingoidea,
- 658 Sphingidae. London: E.W. Classey Ltd. & R.B.D. Publications Inc.
- 38. Schneider CA, Rasband WS, Eliceiri KW. 2012 NIH Image to ImageJ: 25 years of image analysis. *Nat Methods* **9**, 671–675. (doi:10.1038/nmeth.2089)
- 39. Hook TV, Williams EH, Brower LP, Borkin S, Hein J. 2012 A standardized protocol for
- ruler-based measurement of wing length in monarch butterflies, *Danaus plexippus* L.
- 663 (Nymphalidae, Danainae). *Tropical Lepidoptera Research*, 42–52.
- 40. Kennelly D, Grigg J, Tabaru A, Sentak K. 2017 The effects of temperature on *Vanessa* cardui. The Journal of Biological Sciences **3**, 6–8.
- 41. Aprelev P, Gu Y, Burtovyy R, Luzinov I, Kornev KG. 2015 Synthesis and
- characterization of nanorods for magnetic rotational spectroscopy. *Journal of Applied*
- 668 *Physics* **118**, 074901. (doi:10.1063/1.4928401)
- 42. Gu Y, Kornev KG. 2016 Ferromagnetic nanorods in applications to control of the in-
- plane anisotropy of composite films and for *in situ* characterization of the film rheology.
- *Advanced Functional Materials* **26**, 3796–3808. (doi:10.1002/adfm.201504205)
- 43. Wu X-F, Zhang M, Adhikari B, Sun J. 2017 Recent developments in novel freezing and
- thawing technologies applied to foods. Critical Reviews in Food Science and Nutrition
- **57**, 3620–3631. (doi:10.1080/10408398.2015.1132670)
- 675 44. Rindler V, Lüneberger S, Schwindke P, Heschel I, Rau G. 1999 Freeze-drying of red
- blood cells at ultra-low temperatures. *Cryobiology* **38**, 2–15.
- 677 (doi:10.1006/cryo.1998.2143)
- 45. Tolstorebrov I, Eikevik TM, Bantle M. 2016 Effect of low and ultra-low temperature
- applications during freezing and frozen storage on quality parameters for fish.
- International Journal of Refrigeration 63, 37–47. (doi:10.1016/j.ijrefrig.2015.11.003)
- 46. Fedorov A et al. 2012 3D Slicer as an image computing platform for the Quantitative
- Imaging Network. *Magnetic Resonance Imaging* **30**, 1323–1341.
- 683 (doi:10.1016/j.mri.2012.05.001)
- 47. Kawahara AY, Barber JR. 2015 Tempo and mode of antibat ultrasound production and
- sonar jamming in the diverse hawkmoth radiation. *Proceedings of the National Academy*
- *of Sciences* **112**, 6407–6412. (doi:10.1073/pnas.1416679112)
- 48. Paradis E, Schliep K. 2019 ape 5.0: an environment for modern phylogenetics and
- evolutionary analyses in R. *Bioinformatics* **35**, 526–528.
- (doi:10.1093/bioinformatics/bty633)

- 49. Stephens PA, Buskirk SW, del Rio CM. 2007 Inference in ecology and evolution. *Trends in Ecology & Evolution* 22, 192–197. (doi:10.1016/j.tree.2006.12.003)
- 50. Tung Ho L si, Ané C. 2014 A linear-time algorithm for Gaussian and Non-Gaussian trait evolution models. *Systematic Biology* **63**, 397–408. (doi:10.1093/sysbio/syu005)
- 51. R Core Team. 2021 R: A language and environment for statistical computing.
- 52. Rezende EL, Diniz-Filho JAF. 2012 Phylogenetic analyses: Comparing species to infer
 adaptations and physiological mechanisms. *Comprehensive Physiology* 2, 639–674.
 (doi:10.1002/cphy.c100079)
- 53. Burnham KP, Anderson DR. 2004 Multimodel inference: Understanding AIC and BIC in model selection. *Sociological Methods & Research* 33, 261–304.
 (doi:10.1177/0049124104268644)
- 54. Berret J-F. 2016 Microrheology of viscoelastic solutions studied by magnetic rotational spectroscopy. *International Journal of Nanotechnology* 13, 597.
 (doi:10.1504/IJNT.2016.079661)
- 55. Wasserthal LT. 2012 Circulation and thermoregulation. In *Teilband/Part 36, Vol 2:* Morphology, Physiology, and Development (ed N Kristensen), pp. 205–228. Berlin: De
 Gruyter. (doi:10.1515/9783110893724.205)
- Tublitz N. 1989 Insect cardioactive peptides: neurohormonal regulation of cardiac
 activity by two cardioacceleratory peptides during flight in the tobacco hawkmoth,
 Manduca sexta. Journal of Experimental Biology 142, 31–48. (doi:10.1242/jeb.142.1.31)
- 57. Smits AW, Burggren WW, Oliveras D. 2000 Developmental changes in *in vivo* cardiac performance in the moth *Manduca sexta*. *Journal of Experimental Biology* **203**, 369–378. (doi:10.1242/jeb.203.2.369)
- 58. Vogel S. 1996 *Life in Moving Fluids*. Princeton: Princeton University Press. See https://press.princeton.edu/books/paperback/9780691026169/life-in-moving-fluids.
- 59. Revell LJ. 2012 *phytools*: an R package for phylogenetic comparative biology (and other things). *Methods in Ecology and Evolution* 3, 217–223. (doi:10.1111/j.2041-210X.2011.00169.x)
- 60. Lighthill MJ. 1975 Introduction to the scaling of animal locomotion. In Scale Effects in
 Animal Locomotion: Based on the Proceedings of an International Symposium Held at
 Cambridge University, September, 1975 (ed TJ Pedley), pp. 365–404. London and New
 York: Academic Press.
- 61. Weis-Fogh T. 1973 Quick estimates of flight fitness in hovering animals, including novel
 mechanisms for lift production. *Journal of Experimental Biology* 59, 169–230.
 (doi:10.1242/jeb.59.1.169)
- 62. Weis-Fogh T. 1975 Dimensional analysis of hovering flight. In Scale Effects in Animal
 Locomotion: Based on the Proceedings of an International Symposium Held at
 Cambridge University, September, 1975 (ed TJ Pedley), pp. 405–420. London and New
 York: Academic Press.

- 63. Greenewalt CH. 1962 *Dimensional relationships for flying animals*. Washington, DC:
 Smithsonian Miscellaneous Collections.
- 64. Casey TM. 1976 Flight energetics of sphinx moths: power input during hovering flight.
 Journal of Experimental Biology 64, 529–543. (doi:10.1242/jeb.64.3.529)
- 733 65. Casey TM. 1992 Biophysical ecology and heat exchange in insects. *American Zoologist* 32, 225–237. (doi:10.1093/icb/32.2.225)
- 66. O'Connor MP, Spotila JR. 1992 Consider a spherical lizard: Animals, models, and approximations. *American Zoologist* **32**, 179–193. (doi:10.1093/icb/32.2.179)
- 67. Regier JC, Grant MC, Mitter C, Cook CP, Peigler RS, Rougerie R. 2008 Phylogenetic relationships of wild silkmoths (Lepidoptera: Saturniidae) inferred from four protein-coding nuclear genes. *Systematic Entomology* 33, 219–228. (doi:10.1111/j.1365-3113.2007.00416.x)
- 68. Kawahara AY, Mignault AA, Regier JC, Kitching IJ, Mitter C. 2009 Phylogeny and
 biogeography of hawkmoths (Lepidoptera: Sphingidae): Evidence from five nuclear
 genes. PLOS ONE 4, e5719. (doi:10.1371/journal.pone.0005719)
- 69. Kawahara AY. 2007 Molecular phylogenetic analysis of the hawkmoths (Lepidoptera:
 Bombycoidea: Sphingidae) and the evolution of the sphingid proboscis. M.S., University
 of Maryland, College Park, United States -- Maryland. See
 https://www.proquest.com/docview/304850997/abstract/9B6929FEA3DA4BB3PO/1.
- 70. Kingsolver JG, Koehl M a. R. 1985 Aerodynamics, thermoregulation, and the evolution of insect wings: Differential scaling and evolutionary change. *Evolution* **39**, 488–504. (doi:10.1111/j.1558-5646.1985.tb00390.x)
- 71. Beetz S, Holthusen TK, Koolman J, Trenczek T. 2008 Correlation of hemocyte counts with different developmental parameters during the last larval instar of the tobacco hornworm, *Manduca sexta*. *Archives of Insect Biochemistry and Physiology* **67**, 63–75. (doi:10.1002/arch.20221)
- 72. Stoepler TM, Castillo JC, Lill JT, Eleftherianos I. 2013 Hemocyte density increases with developmental stage in an immune-challenged forest caterpillar. *PLOS ONE* 8, e70978.
 757 (doi:10.1371/journal.pone.0070978)

758